Monitoring scan asymmetry of microwave humidity sounding channels using simultaneous all angle collocations (SAACs)

Article

Published Version

JOURNAL OF GEOPHYSICAL RESEARCH: ATMOSPHERES, VOL. 118, 1536–1545, doi:10.1002/jgrd.50154, 2013

Monitoring scan asymmetry of microwave humidity sounding channels using simultaneous all angle collocations (SAACs)

Viju O. John,[1] Gerrit Holl,[2] Nigel Atkinson,[3] and Stefan A. Buehler[2]

Received 12 July 2012; revised 18 November 2012; accepted 1 January 2013; published 14 February 2013.

[1] Simultaneous all angle collocations (SAACs) of microwave humidity sounders (AMSU-B and MHS) on-board polar orbiting satellites are used to estimate scan-dependent biases. This method has distinct advantages over previous methods, such as that the estimated scan-dependent biases are not influenced by diurnal differences between the edges of the scan and the biases can be estimated for both sides of the scan. We find the results are robust in the sense that biases estimated for one satellite pair can be reproduced by double differencing biases of these satellites with a third satellite. Channel 1 of these instruments shows the least bias for all satellites. Channel 2 has biases greater than 5 K, thus needs to be corrected. Channel 3 has biases of about 2 K and more and they are time varying for some of the satellites. Channel 4 has the largest bias which is about 15 K when the data are averaged for 5 years, but biases of individual months can be as large as 30 K. Channel 5 also has large and time varying biases for two of the AMSU-Bs. NOAA-15 (N15) channels are found to be affected the most, mainly due to radio frequency interference (RFI) from onboard data transmitters. Channel 4 of N15 shows the largest and time varying biases, so data of this channel should only be used with caution for climate applications. The two MHS instruments show the best agreement for all channels. Our estimates may be used to correct for scan-dependent biases of these instruments, or at least used as a guideline for excluding channels with large scan asymmetries from scientific analyses.

Citation: John, V. O., G. Holl, N. Atkinson, and S. A. Buehler (2013), Monitoring scan asymmetry of microwave humidity sounding channels using simultaneous all angle collocations (SAACs), *J. Geophys. Res. Atmos.*, *118*, 1536–1545, doi:10.1002/jgrd.50154.

1. Introduction

[2] Tropospheric humidity measurements are important for monitoring weather and climate. Global microwave humidity measurements from satellites are available since the early 1990s. These measurements have the advantage of almost all-weather availability [e.g., *John et al.*, 2011] compared to their infrared counterparts. Microwave humidity sounders onboard polar orbiting satellites such as Advanced Microwave Sounding Unit (AMSU-B) and Microwave Humidity Sounder (MHS) are cross-track scanning radiometers with equal number of samples on either side of nadir. Scan symmetry is expected, but for various reasons, for example, interference with onboard data transmitters, this symmetry is often broken [*Atkinson*, 2001]. Therefore scan-dependent biases exist, compromising the use of the data in scientific analyses.

[3] Often, inter-calibration efforts [*Iacovazzi and Cao*, 2007; *Wang et al.*, 2007; *Goldberg et al.*, 2011; *John et al.*, 2012b] use only near-nadir measurements and assume the biases estimated for nadir are applicable for all viewing angles. However, as stated above, this is not often true and scan asymmetries must be taken into account while inter-calibrating cross-track scanning instruments.

[4] There are only a few studies that address scan asymmetries of atmospheric sounders. For example, for the AMSU-A sensor, which is dedicated to temperature measurements, such asymmetries have been reported by *Weng et al.* [1999, 2003]. They proposed that the asymmetry could have resulted from several causes such as errors in polarization angle alignment and antenna pointing angle. The initial analyses for NOAA-15 and NOAA-16 AMSU-A showed that an adjustment of -1.5° to the instrument polarization angle was needed to remove the asymmetry. They used radiative transfer simulations of AMSU-A measurements using surface and atmospheric parameters from the NCEP global data assimilation system.

[5] *Buehler et al.* [2005] have shown scan asymmetry for AMSU-B instruments on board NOAA-15 (N15), N16, and N17 satellites. They subtracted one side of a scan from the other using 3 months of data so that random asymmetries related to weather would be averaged out. Although their method was simple, *Buehler et al.* [2005] could correctly identify large biases in some of the AMSU-B channels. One

[1]Met Office Hadley Centre, Exeter, United Kingdom.
[2]Division of Space Technology, Department of Computer Science, Electrical and Space Engineering, Luleå University of Technology, Kiruna, Sweden.
[3]Met Office, Exeter, United Kingdom.

Corresponding author: V. O. John, Met Office Hadley Centre, Exeter, UK. (viju.john@metoce.gov.uk)

2169-897X/13/10.1002/jgrd.50154

disadvantage of their method is that it is not possible to identify which side of the scan has the bias.

[6] An important aspect is the solar/antisolar sides of the scan. Even for a perfect instrument, one should expect asymmetry if the quantity measured has a diurnal cycle and the instrument is carried on a sun-synchronous orbit, as one side of the scan is always toward the sun and the other side away from the sun, so there should be a small diurnal effect (there will be typically 1.5 h difference between scan edges at the equator). With previous methods, the diurnal cycle effect cannot be separated from the instrumental effect.

[7] In this study, simultaneous all-angle collocations (SAACs) of microwave humidity sounders on different satellites are used to estimate scan-dependent biases. The details of SAACs will be given in section 3.1 and in this method diurnal cycle effects are not confused with the estimated scan-dependent biases. Another advantage of this study is that the biases on both sides of the scan can be estimated. The aim of this study is to document the biases which can be used as a guideline to judge the utility of data from AMSU-Bs and MHSs for scientific applications.

2. Data and Method

2.1. Microwave Humidity Sounders

[8] In this study we used data from AMSU-B [*Saunders et al*., 1995] and MHS [*Bonsignori*, 2007]. Instrument and data descriptions provided here are based on other articles, for example, *John and Buehler* [2004]. AMSU-B is a cross-track line scanning, passive, total power microwave radiometer with five channels. Three channels are centered on the strong water vapor line at 183.31 GHz with sidebands located at ±1.00, ±3.00, and ±7.00 GHz away from the line center and are called Channels 3, 4, and 5, respectively. The remaining two channels are window channels centered at 89 and 150 GHz. Each swath consists of 90 samples with a sampling distance of 1.10° resulting in a total viewing angle range of −48.95° to +48.95° around nadir [*Saunders et al*., 1995]. The swath width is about 2300 km and the footprint size ranges from $20 \times 16\,km^2$ at nadir to $64 \times 27\,km^2$ at the edge of the scan. We call scan positions 1–45 "the left" side of the scan and scan positions 46–90 the "right side" of the scan. Scan position 1 is at the left edge of the scan and scan position 90 is at the right edge of the scan. We call the viewing angles "negative" for the left side of the scan and "positive" for the right side of the scan.

[9] The MHS is similar to AMSU-B except that Channel 2 is at 157 GHz and Channel 5 has only the upper sideband at 183.31 + 7.00 GHz. These changes introduce state-dependent biases for these channels [e.g., *John et al*., 2012a].

[10] Level 1b [*Goodrum et al*., 2007] data of AMSU-B and MHS were obtained from the NOAA/CLASS digital library. Level 1b files contain quality controlled raw instrument counts. Geographical and operational calibration information is also included in the files. The ATOVS and AVHRR Processing Package (AAPP) [*Labrot et al*., 2011] was used to convert level 1b data to level 1c data. During this process, the calibration coefficients are applied to the instrument counts to obtain antenna temperature and this is then converted to brightness temperatures by applying an antenna pattern correction [*Hewison and Saunders*, 1996]. Corrections for Radio Frequency Interference (RFI which is discussed in detail in *Atkinson* [2001]) are also done during the conversion to level 1c.

[11] The AMSU-B and MHS data have been used for a variety of hydrological research applications such as retrieving humidity profiles, liquid and cloud ice water paths, for monitoring climate modes like monsoon, and assimilating into numerical weather prediction models [*Karbou et al*., 2005; *Eymard et al*., 2010; *Ferraro et al*., 2005; *Liu and Weng*, 2005; *Andersson et al*., 2007].

2.2. Collocation Methodology

[12] The collocation methodology is described in detail in *Holl et al*. [2010] and John *et al*. [2012a], implemented with a publicly available, highly flexible toolkit for the collocation of arbitrary satellite sensor data records. A brief description of the methodology is provided here: For each data file of the primary satellite, files of secondary satellites with a time overlap are identified. Within the time overlap between these primary and secondary files, all footprints are gridded on an equirectangular lat/lon grid. Within each grid cell, distances are calculated between all primary footprints and all secondary footprints within the same or a nearby grid cell, where "nearby" is a function of latitude, grid cell size, and collocation distance. For all distances less than the collocation distance, the time interval is calculated. Every pair where distance and time interval are less than a prescribed maximum (15 km, 15 min) are stored as collocations. The resulting data set is available for public use and was used earlier by *John et al*. [2012a]. In the present study, a subselection within this dataset is made as described below.

2.3. Analysis Methodology

[13] Sensitivity analyses were done by *John et al*. [2012a] on the impact of distance and time threshold criteria for selecting the collocations on the estimated bias based on the uncertainty of the biases (Figure 3 of *John et al*. [2012a]). They found that, to overcome spatial inhomogeneity, only those pixel pairs whose centers are closer than 5 km, which is less than one third of the 16.3 km pixel diameter at nadir, are to be used in the analyses. This threshold then increases linearly to 15 km at the edge of the scan to be consistent with the increase in size of the footprint. We discard any measurements with time differences exceeding 300 s, to avoid changes in scene properties such as clouds, which is again based on findings by *John et al*. [2012a]. Only those pixel pairs with the same field of view are used to avoid errors arising from the limb effect. For example, scan position 1 of one satellite is only paired with scan position 1 of the second satellite. Collocations over both land and ocean are used throughout this study.

[14] Using those pixel pairs which satisfied these criteria, we first calculate differences in brightness temperatures and then derive the mean difference or bias ($\Delta\bar{T}_B$) and the standard deviation of the differences ($\sigma_{\Delta T_B}$). In order to have robust statistics, data are collected and combined for a month to calculate these quantities. We then calculate standard errors of mean values, namely $\sigma_{\Delta T_B}$ divided by the square root of the number of collocations, which may be plotted as error bars when biases are presented.

[15] The SAACs occur normally in polar regions and intersatellite biases are often state dependent [e.g., *John et al*., 2012a] and therefore the estimated biases may be slightly

biased in moist regions, but the general scan dependency of biases remains the same as discussed later in more detail in section 3.2. *John et al.* [2012a] provide more details on latitude dependence of biases.

[16] Both liquid and ice clouds affect these channels [*Sreerekha et al.*, 2008]. However, in polar conditions, it is difficult to differentiate between clouds and the surface. Due to our stringent spatio-temporal collocation criteria, it is assumed that measurements from both instruments are affected by clouds in a similar way, so the measurements were not screened for them.

3. Results and Discussion

3.1. Simultaneous All Angle Collocations (SAACs)

[17] The number of SAACs per month is a function of (1) primary satellite, (2) secondary satellite, (3) maximum time interval, (4) maximum distance, (5) viewing angle, (6) latitude, and (7) time. A brief summary of the most important patterns in this eight-dimensional dependence is given below. Figure 1 illustrates the number of SAAC per month for 10 satellite pairs since 2001, as well as the latitude range covered. The figure shows that many satellite pairs have around 4000–8000 polar-only SAACs/month using the criteria described in section 2.3. Two pairs have periods with global occurrences of SAAC: N15–N16 (shown in the upper panel of Figure 2) and MA–N17, a fact that is exploited by looking at the latitudinal dependence of the bias pattern (see below). Some satellite pairs, such as N17–N15, have SAACs only intermittently, with many for some months and none at all for others. This reduces the usability of this pair for analysis. Since the largest permitted distance and time increases with viewing angle, so does the number of SAAC. Therefore, the larger the viewing angle, the more the number of collocations as shown in the lower panel of Figure 2.

3.2. Do Bias Patterns Change With Latitude?

[18] Most of the time, SAACs occur only in polar regions [*Cao et al.*, 2004] and as discussed in *John et al.* [2012a], the biases vary with latitude due to the dependence of biases on scene radiances [*Shi et al.*, 2008; *Shi and Bates*, 2011]. Therefore it is important to evaluate the patterns of scan asymmetry for different latitude bands. We have selected the N16–N15 pair during August 2008 to evaluate this. During this time period, this pair has global collocations owing to similar equator crossing times resulting from orbit drift. The collocations are binned into nine latitude bands with 20° width. The results are shown for Channel 5 in Figure 3 as an example. It can be seen that there is about 2 K difference between Arctic and Antarctic collocations, which is consistent with *John et al.* [2012a], but the scan dependency of bias is similar for all latitude bands. This is an encouraging result because even if there are differences in the magnitude of bias from one latitude band to other, the bias patterns remains the same and thus we can utilize SAACs with limited latitude coverage for monitoring scan asymmetries of these channels.

3.3. Scan-Dependent Biases

[19] In the following subsections, we discuss the scan-dependent biases for the humidity sounders, channel by channel. All possible satellite pairs are shown so that it is possible to determine which satellite has scan asymmetry.

[20] Ideally, one should present biases of each satellite for all months available. That is too much information and too many figures to present in the paper. To present the results in a non-cluttered manner (Figures 4–8), we show only averages of these monthly biases for two periods; 2001–2005 and 2006–2010. We are aware that multi-annual averaging of the biases will conceal fine features and large magnitudes for some cases, but the detailed data show that patterns of scan asymmetry generally remain unchanged. The difference in bias

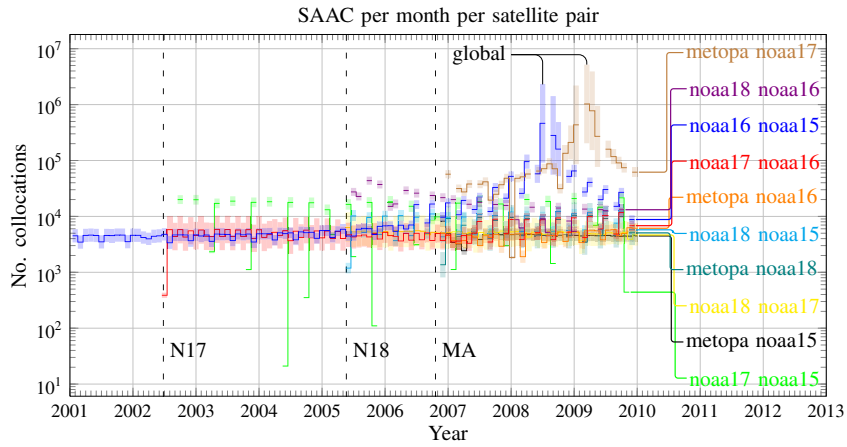

Figure 1. Time series showing the number of SAAC for 10 satellite pairs in the period 2001–2010. The opaque lines show the total number of SAACs for a particular month. The vertical axis is logarithmic, and no value is plotted for months in which no SAACs occur at all. The lighter colored filled area around each line gives an indication of the latitude range covered by the SAACs for a particular month; the wider this filled area, the larger the range of latitudes covered. Two periods where global SAACs exist are marked explicitly. The dashed vertical lines show the launch dates of NOAA-17, NOAA-18 and MetOp-A, respectively. Each minor tick corresponds to a month.

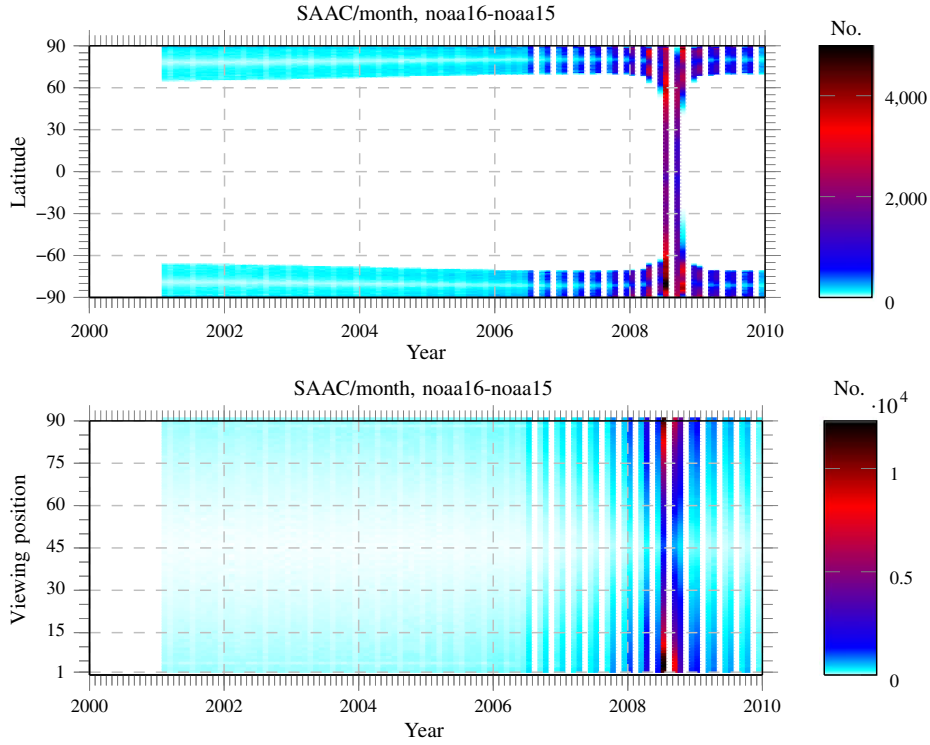

Figure 2. Number of SAACs for N16–N15 pair for 2001–2010 versus (upper panel) latitude and (lower panel) viewing position.

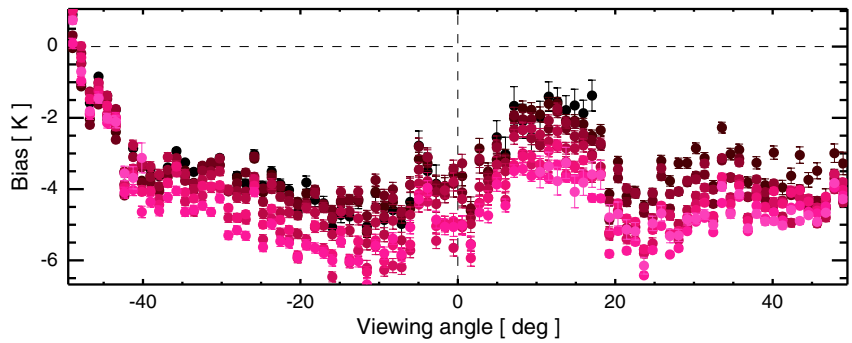

Figure 3. Scan-dependent biases for Channel 5 of N16–N15 pair during 2008-08 when global biases were available for this satellite pair. The biases are shown for different latitude bands in different colors (the darkest color denotes southern most latitude bin, and the lightest color denotes the northern most latitude bin). Width of each latitude band is 20°. The vertical bars represent standard errors of the biases.

between the two periods can be considered as an indication of time-varying biases. These multi-annual averages are calculated by weighting monthly mean values with $\frac{N}{\sigma^2}$, where N is the number of collocation per month and σ is the standard deviation of monthly differences. Weighted errors of the multi-annual means are shown as vertical bars in Figures 4–8.

[21] Table 1 shows the number of months in each year that bias data are available for each satellite pair, and Figure 1 summarizes the occurrence of SAACs. Because SAACs occur only intermittently for the N17–N15 pair, yielding fewer months in a year with bias values, we have not included this pair in any of the subsequent Figures. Biases are always calculated as newer satellite minus older satellite. Launch dates of the satellites are also given in the caption of Table 1 and in Figure 1.

3.3.1. Channel 1

[22] This channel is centered at 89 GHz and is a surface sensitive channel at all weather conditions [*John et al.*, 2012a]. Figure 4 shows the scan-dependent biases for Channel 1. Average biases for 2001–2005 and 2006–2010 are shown.

[23] Bias patterns are similar for N15 against all other satellites. The left edge of the scan shows a negative bias which is up to −1 K during 2006–2010 against N16. The right edge of the scan also shows a small negative bias. Biases of N15 against N16 between 2001–2005 and 2006–2010 vary from 0.2 to 0.3 K for most viewing angles. Biases of N15 against MA are flat within ±35° viewing angles. Overall, N15 brightness temperatures are colder at the middle of the scan and warmer at the edges compared to all other satellites.

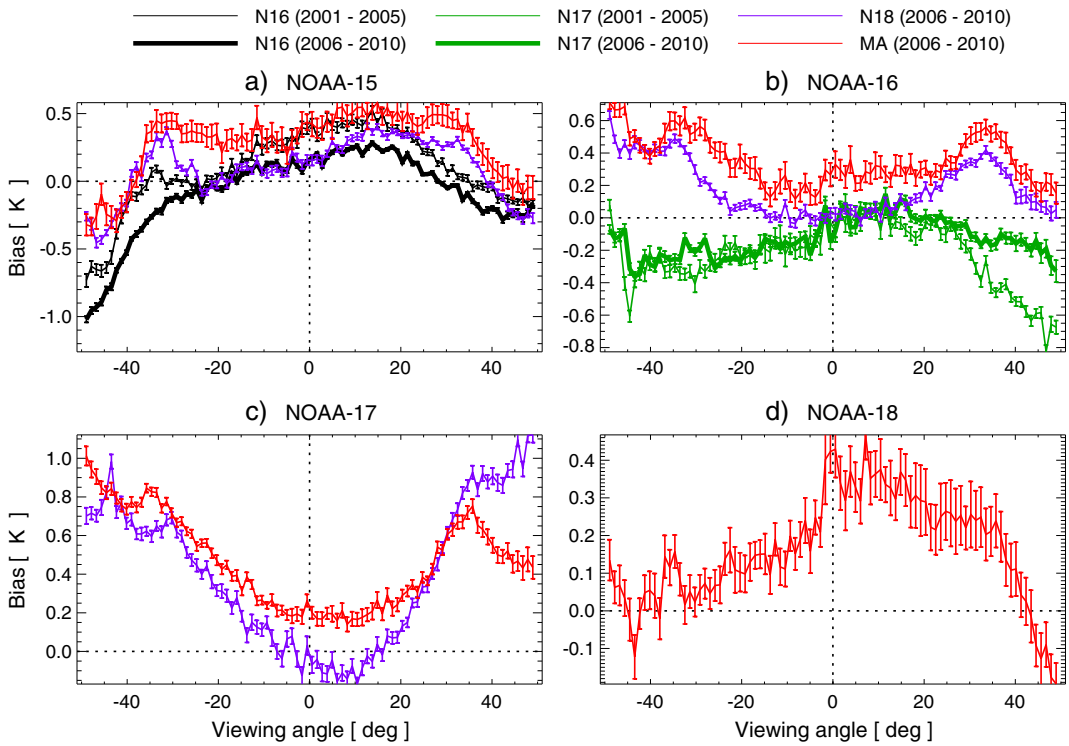

Figure 4. Scan-dependent biases of Channel 1 (89 GHz) for (a) NOAA-15, (b) NOAA-16, (c) NOAA-17, and (d) NOAA-18 compared to other satellites. In each sub-panel, data for the particular satellite are subtracted from other satellites when sufficient data are available. We show mean biases and their errors for 2001–2005 and 2006–2010 periods when available, instead of individual months, to avoid clutter. Note, for example, that N17 was launched only in 2002–2006 therefore, 2001–2005 period for that satellite will have only three and a half years of data. Numbers of months for which data are available for each satellite pair are given in Table 1. *Y* axis range of each panel is different.

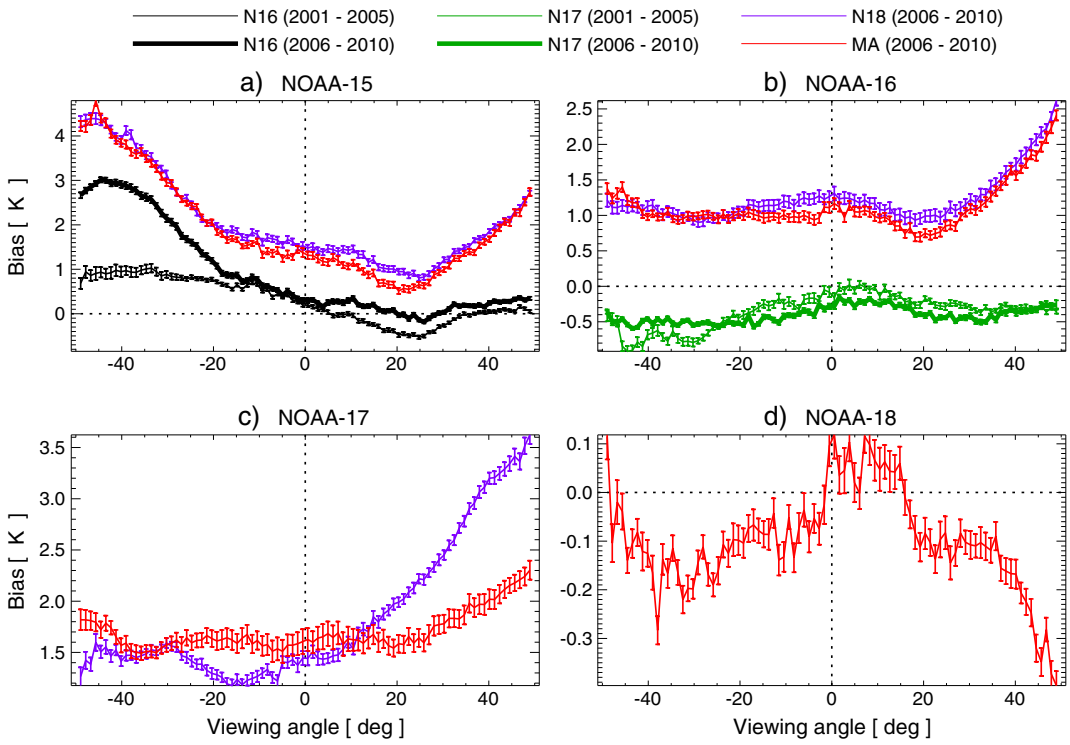

Figure 5. As in Figure 4 but for Channel 2. This channel is at 150 GHz on AMSU-B and at 157 GHz on MHS.

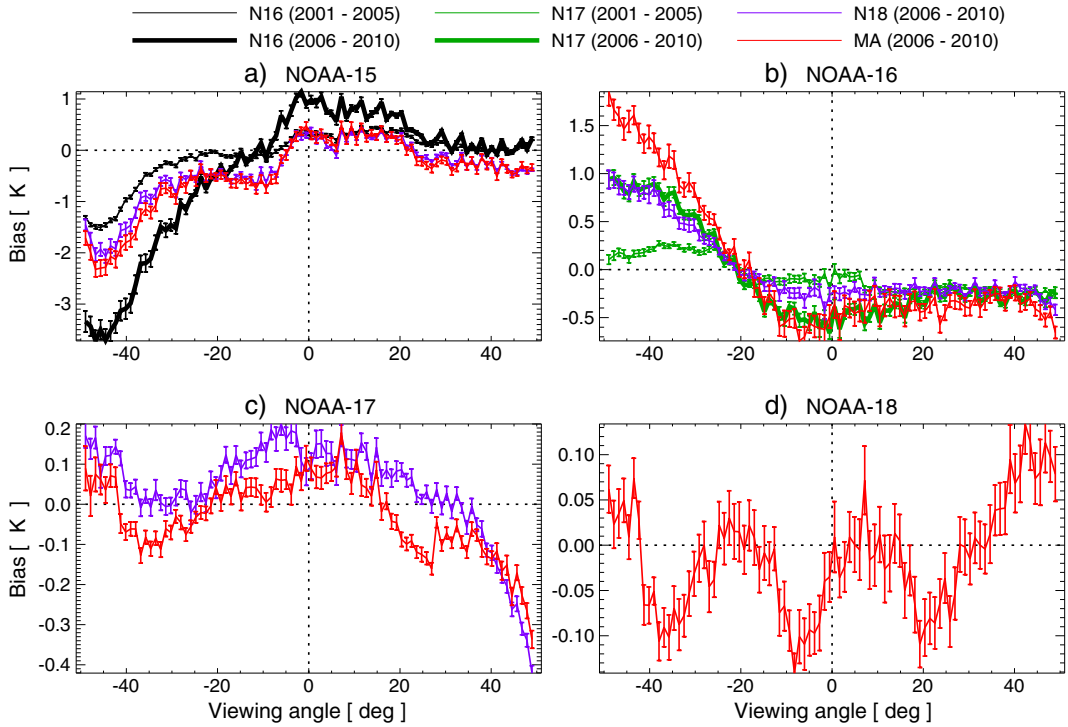

Figure 6. As in Figure 4 but for Channel 3 (183.31 ± 1.00 GHz).

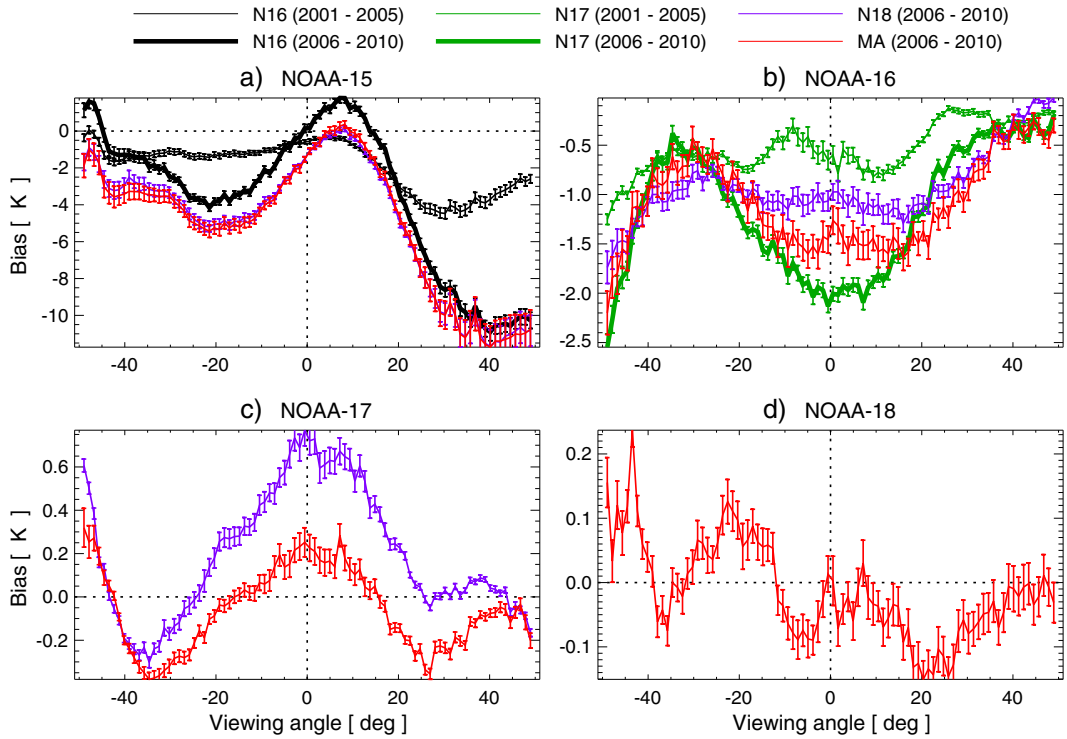

Figure 7. As in Figure 4 but for Channel 4 (183.31 ± 3.00 GHz).

[24] The N16 biases against N17 show no difference between the two time periods except outside 30° on the right side of the scan. The bias patterns of N16 against N18 and MA are mostly similar.

[25] The N17 shows significant scan-dependent biases compared to N18 and MA. Biases are close to zero compared to N18 and about −0.4 K compared to MA near nadir, but the biases increase away from nadir on both sides. This is the reason why N16 biases compared to N17 are different from those compared to N18 and MA.

[26] As expected from previous discussions, MA is warmer than N18 for most of the viewing angles except

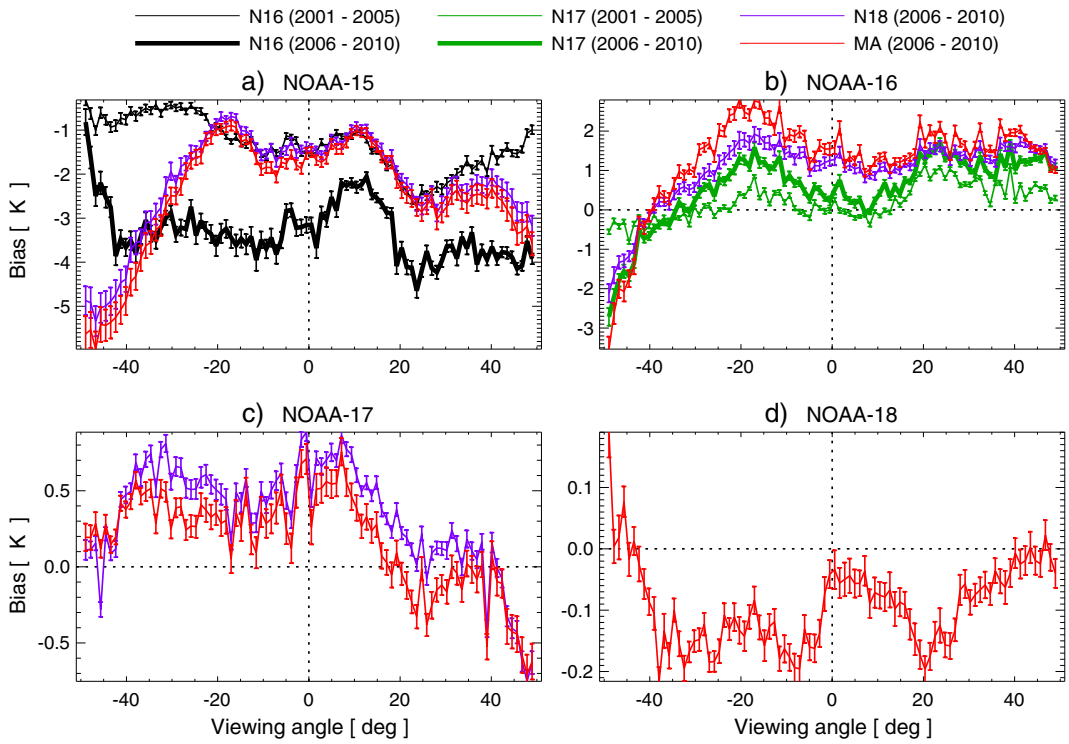

Figure 8. As in Figure 4 but for Channel 5. This channel is at 183.31 ± 7.00 GHz on AMSU-B and at 183.31 + 7.00 GHz on MHS.

Table 1. Number of Months in a Year Data Are Available for All Viewing Angles[a]

	2001	2002	2003	2004	2005	2006	2007	2008	2009	2010
N16-N15	12	12	12	12	12	12	12	12	12	12
N17-N15	-	2	3	4	6	6	4	4	4	3
N18-N15	-	-	-	-	8	12	12	12	12	12
MA-N15	-	-	-	-	-	2	12	12	12	11
N17-N16	-	6	12	12	12	12	12	12	12	12
N18-N16	-	-	-	-	4	6	6	8	5	6
MA-N16	-	-	-	-	-	1	12	12	12	12
N18-N17	-	-	-	-	8	12	12	12	12	12
MA-N17	-	-	-	-	-	3	11	10	9	6
MA-N18	-	-	-	-	-	2	12	12	12	8

[a]N15 was launched in May 1998, N16 was launched in September 2000, N17 was launched in June 2002, N18 was launched in May 2005, and MA was launched in October 2006. Note that the local oscillator of Channels 3–5 failed on N17 in January 2010, so there are no collocations for these N17 channels in 2010.

for the edge of the scans. This bias pattern shown in panel d can be obtained from differencing the results shown in Figure 4c ((MA-N18) ~ (MA-N17) – (N18-N17)). This is another encouraging result that double differences of two satellite pairs can reproduce the bias patterns of another pair, which proves that the bias patterns deduced from this method are not sampling fluctuations.

3.3.2. Channel 2

[27] The center frequency of this Channel is slightly different on AMSU-B and MHS; it has changed from 150 to 157 GHz. Biases thus arising depend on surface and atmospheric conditions. For example, *John et al.* [2012a] showed that under dry conditions, MHS measurements are warmer than AMSU-B ones. AMSU-Bs are on board N15, N16, and N17. MHSs are on board N18 and MA.

[28] Scan-dependent biases of Channel 2 are shown in Figure 5. Unlike Channel 1, this channel shows large biases. One thing that is evident in Figures 5a and 5b is that biases compared to N18 and MA are about 1.5 K more than biases compared to N16 and N17. This is due to the center frequency difference between AMSU-B and MHS.

[29] The N15 shows colder biases more at the left edge of the scan compared to all other satellites and this bias has been growing over time, which is clear from the difference in bias between the two time periods against N16. Biases decrease to about 25° on the right side of the scan and then starts to increase.

[30] The N16 brightness temperatures on average are about half a Kelvin warmer than N17 brightness temperatures for all angles during 2006–2010, thus no significant scan-dependent biases are seen for this channel during this time period. However, during 2001–2005 there are scan-dependent biases. N16 biases against MA and N18 are independent of viewing angles except for the angles greater than 20° on the right side of the scan.

[31] The N17 also show increasing biases with viewing angle on the right side of the scan compared to N18 and MA outside of about 20° and these cold biases are about 2–3 K at the right edge of the scan. This indicates either all AMSU-Bs (N15, N16, N17) or all MHSs (N18, MA) have biases at the right side of the scan.

[32] The MA-N18 pair shows the best agreement for this channel, and the biases are within ±0.4 K.

3.3.3. Channel 3

[33] This channel is sensitive to upper tropospheric humidity (UTH) which is an important climate variable, but not very well simulated by current climate models [e.g., *John and Soden*, 2007]. Therefore this channel is of high interest to

the climate community [e.g., *Xavier et al*., 2010]. Brightness temperatures measured by this channel are exponentially related to UTH and 1 K error in brightness temperature corresponds to 7% relative error in UTH [*Buehler and John*, 2005]. Scan-dependent biases of Channel 3 are shown in Figure 6.

[34] The left side of the N15 scan shows significant biases compared to all other satellites. The biases are time-varying with differences of 3 K between 2001–2005 and 2006–2010 against N16.

[35] The N16 shows very small biases against N17 during 2001–2005, but the biases have increased during 2006–2010 by about a Kelvin at the left edge of the scan. The difference of N16–N15 biases for 2006–2010 to those of N18 and MA can be attributed to this relative cooling of N16.

[36] The N17 biases against N18 and MA show similar patterns, but the biases are within ±0.4 K.

[37] The N18 and MA satellite show very close agreement for this channel which is good news for inter-calibration efforts for this channel.

3.3.4. Channel 4

[38] This channel is sensitive to the mid tropospheric humidity which is also an important climate variable to monitor due to its contribution to the water vapor feedback. Also, it monitors and evaluates convective moistening in climate models [*Xavier*, 2012]. However, this is the channel with the largest biases of the microwave humidity sounding channels, which can be seen in Figure 7.

[39] Channel 4 on N15 is known to have suffered from Radio Frequency Interference (RFI; see also section 3.5) and as a result biases are as large as 12 K and time varying. For individual months, the biases are sometimes more than 30 K (not shown). The right end of the scan has largest biases, unlike other channels.

[40] The N16 also shows significant and time-varying biases. The left edge of the scan has more than 2 K and the middle of the scan has about 1–2 K biases during 2006–2010.

[41] The N17 shows similar bias patterns against N18 and MA. The left edge and middle of the scan has about 0.6 K cold bias in N17 brightness temperatures compared to N18, but the biases in the middle of the scan are smaller compared to MA.

[42] The MA–N18 is the only pair with small biases, but all other pairs have significant biases. This implies that this channel on all AMSU-B instruments must be used with caution for climate monitoring.

3.3.5. Channel 5

[43] This channel is sensitive to the lower tropospheric humidity, but with significant contribution from the surface under dry conditions. Channel configurations have been slightly changed from AMSU-B to MHS; AMSU-B has two passbands at 183.31 ± 7.00 GHz while MHS has only one passband at 183.31 + 7.00 GHz. The 183.31 + 7.00 GHz passband has a slightly higher absorption compared to the 183.31–7.00 GHz. The biases arising from this depend on atmospheric and surface conditions [*John et al*., 2012a].

[44] The N15 shows significant warm bias for all viewing angles and they are increasing over time. The difference in bias patterns of N16–N15 to N18–N15 and MA–N15 is due to the biases of the N16 channel which is shown in Figure 7b.

[45] The N17 also show significant biases and scan asymmetry. MA and N18 show good agreement with biases within ±0.2 K.

3.4. Time Evolution of Biases

[46] For some of the channels, for example, the three humidity sounding channels of N15, the biases are increasing over time as depicted in previous figures. However, it is important to understand whether the biases show any seasonal variations.

[47] As an example, Figure 9 shows the time series of Channel 5 biases of N16–N15 pair for the first viewing angle from the left edge. It can be seen that the biases are not decreasing monotonically with time as one would envisage from Figure 8. It shows relatively smaller variations until mid 2008, but after that very large oscillations are seen. This surely illustrates an instrumental problem which is similar to what is shown in Figures 2 and 4 of *Zou and Wang* [2011]. They showed large changes in instrument temperatures of AMSU-A leading to variations in the spacecraft thermal emission affecting the signals in the antenna sidelobe views of Earth and calibration targets. Therefore we are planning to study instrumental characteristics of humidity sounders to improve understanding of these biases.

[48] Because of this time dependence in biases, one has to use biases and their error estimates for satellite pairs for individual months. These data will be available on request. Also, it is planned to continually update these data sets.

3.5. Discussion

[49] As discussed in detail in *Atkinson* [2001], soon after the launch of the first AMSU-B in orbit, it was noticed that AMSU-B data are contaminated due to radio frequency interference (RFI) from data transmitters. This is the main reason for large scan-dependent biases, particularly for Channels 2, 4, and 5 of N15. Ground-based investigations showed that the interference was due to pickup in the receiver video amplifier. For N16 and N17, improved shielding was applied to this area of the receiver, and this resulted in much smaller RFI post-launch. RFI corrections for level 1b instrument data were generated based on in-orbit tests in which the interfering transmitters were cycled on and off. The corrections are documented in Appendix M of *Goodrum et al*. [2007]. Originally the intention was that the corrections would be updated regularly, but in practice they have been fixed since 2001, and all the data analyzed in this paper use constant corrections.

[50] As the instruments have aged, the receiver gains for Channels 3–5 on N15 and N16 have fallen, as seen in Figure 10. The gain reduction is strongest for N16 and is likely to be due to degradation of the receiver front-end (mixer and/or local oscillator). Since the RFI originates in the back end of the receiver, this means that RFI tends to

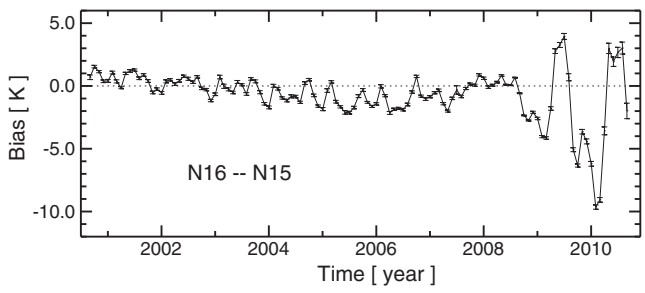

Figure 9. Time series of biases of N16–N15 pair for the leftmost scan position of Channel 5. The vertical bars represent standard errors of the biases.

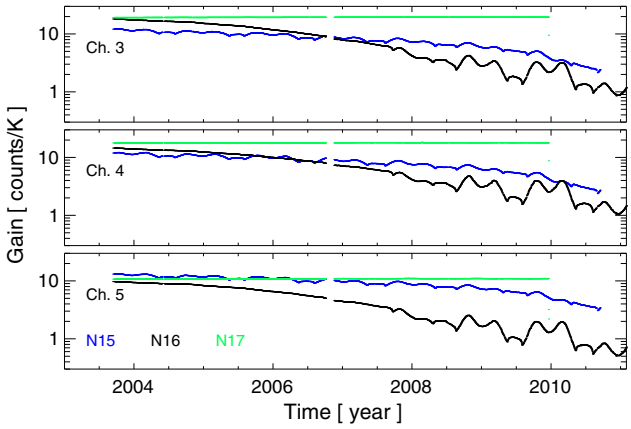

Figure 10. Time series of instrument gains for Channels 3–5 of AMSU-B instruments. Note the *y* axis is in log-scale.

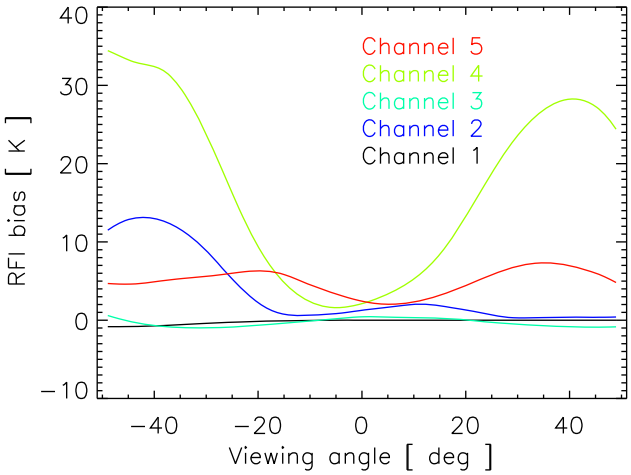

Figure 11. Radio frequency interference (RFI) corrections applied to N15 AMSU-B channels in March 2001.

become more dominant as the instruments age. In the case of N16, no RFI was detected during the post-launch commissioning period—i.e., any RFI was masked by natural atmospheric variability. This is confirmed by Figure 7b, which shows a relatively small (<1 K) Channel 4 cross-scan bias with respect to N17 during the period 2001–2005. However, by 2006–2010, the cross-scan bias has increased up to ~3 K. This is consistent with the reduction in gain for N16 Channel 4, shown in Figure 10. It raises the interesting possibility that end-of-life bias measurements (when the instrument is too noisy to be usable for NWP) are still useful for understanding biases that were present earlier in the life of the instrument.

[51] It has to be noted that the magnitude of RFI biases are very large as shown in Figure 11 which depicts RFI biases estimated for N15 AMSU-B data in March 2001 which is when the RFI corrections in the level 1b files were last updated.

4. Summary and Conclusions

[52] In this study we have used simultaneous all angle collocations (SAACs) of NOAA and MetOp polar orbiting satellites to assess scan-dependent biases of microwave humidity sounders on board these satellites. Although SAACs mostly occur at polar latitudes, we have used data from global collocations to illustrate that bias patterns remain similar at all latitude bands.

[53] We have shown that some of the AMSU-B and MHS channels have large scan asymmetries. For example, Channel 4 of AMSU-B on N15 has the largest scan asymmetry; about 10 positions on the right edge of the scan suffer more than 15 K bias during 2006–2010. The bias estimated for one satellite pair can be reproduced by double differencing biases of these satellites with a third satellite in most cases. This shows the fidelity of the biases estimated using SAACs.

[54] Humidity sounding channels (Channels 3–5) of N15 and N16 show significant scan-dependent biases after 2006. Therefore bias correction using only near-nadir measurements is not sufficient for these channels. These channels on N17 also have scan-dependent biases, but not as large as in the cases of N15 and N16. MHS instruments on N18 and MA show the best agreement and very little scan-dependent bias correction is needed for their channels.

[55] Time evolution of the biases for some satellites shows seasonal patterns associated with instrument temperature changes due to sun angle variations which is shown in *Zou and Wang* [2011].

[56] We propose to use SAACs of other instruments to monitor scan-asymmetries in their data. We plan to extend the application of SAACs to MHS on N19 (data available only from late 2009) and to SSM-T/2 which is another humidity sounding instrument.

[57] **Acknowledgments.** We thank David Parker and Roger Saunders and three anonymous reviewers for valuable comments. Viju John was supported by the Joint DECC/Defra Met Office Hadley Centre Climate Programme (GA01101), the UK JWCRP, and EUMETSAT CMSAF. This work contributes to COST Action ES604–Water Vapor in the Climate System (WaVaCS). Thanks to Lisa Neclos of the NOAA CLASS for AMSU-B and MHS Level-1b data, EUMETSAT NWP-SAF for the AAPP software to process the data.

References

Andersson E., E. Holm, P. Bauer, A. Beljaars, G. A. Kelly, A. P. McNally, A. J. Simmoons, J.-N. Thpaut, and A. M. Tompkins (2007), Analysis and forecast impact of the main humidity observing systems, *Q. J. R. Meteorol. Soc.*, *133*, 1473–1485, doi:10.1002/qj.112.

Atkinson N. C. (2001), Calibration, monitoring and validation of AMSU-B, *Adv. Space Res.*, *28*(1), 117–126.

Bonsignori R. (2007), The Microwave Humidity Sounder (MHS): In-orbit performance assessment, in Proc. SPIE, 67440A, vol. 6744, doi:10.1117/12.737986.

Buehler S. A., and V. O. John (2005), A simple method to relate microwave radiances to upper tropospheric humidity, *J. Geophys. Res.*, *110*, D02110, doi:10.1029/2004JD005111.

Buehler S. A., M. Kuvatov, and V. O. John (2005), Scan asymmetries in AMSU-B data, *Geophys. Res. Lett.*, *32*, L24810, doi:10.1029/2005GL024747.

Cao C., M. Weinreb, and H. Xu (2004), Predicting simultaneous nadir overpasses among polar-orbiting meteorological satellites for the intersatellite calibration of radiometers, *J. Atmos. Oceanic Technol.*, *21*, 537–542.

Eymard L., F. Karbou, S. Janicot, N. Chouaib, and F. Pinsard (2010), On the use of Advanced Microwave Sounding Unit-A and -B measurements for studying the monsoon variability over West Africa, *J. Geophys. Res.*, *115*, D20115, doi:10.1029/2009JD012935.

Ferraro R. R., F. Weng, N. C. Grody, L. Zhao, H. Meng, C. Kongoli, P. Pellegrino, S. Qiu, and C. Dean (2005), NOAA operational hydrological products derived from the advanced microwave sounding unit, *IEEE T. Geosci. Remote*, *43*(5), 1036–1049.

Goldberg M., et al. (2011), The global space-based inter-calibration system, *Bulletin of the American Meteorological Society*, *92*(4), 467–475, doi:10.1175/2010BAMS2967.1.

Goodrum G., K. B. Kidwell, and W. Winston (2007), NOAA KLM user's guide, Tech. rep., National Environmental Satellite, Data, and Information Services (NESDIS).

Hewison T. J., and R. W. Saunders (1996), Measurements of the AMSU-B antenna pattern, *IEEE T. Geosci. Remote*, *34*(2), 405–412, doi:10.1109/36.485118.

Holl G., S. A. Buehler, B. Rydberg, and C. Jiménez (2010), Collocating satellite-based radar and radiometer measurements—Methodology and usage examples, *Atmos. Meas. Tech.*, *3*, 693–708, doi:10.5194/amt-3-693-2010.

Iacovazzi Jr. R. A., and C. Cao (2007), Quantifying EOS aqua and NOAA POES AMSU-A brightness temperature biases for weather and climate applications utilizing the SNO method, *J. Atmos. Oceanic Technol.*, *24*, 1895–1909, doi:10.1175/JTECH2095.1.

John V. O., and S. A. Buehler (2004), The impact of ozone lines on AMSU-B radiances, *Geophys. Res. Lett.*, *31*, L21108, doi:10.1029/2004GL021214.

John V. O., and B. J. Soden (2007), Temperature and humidity biases in global climate models and their impact on climate feedbacks, *Geophys. Res. Lett.*, *34*, L18704, doi:10.1029/2007GL030429.

John V. O., G. Holl, R. P. Allan, S. A. Buehler, D. E. Parker, and B. J. Soden (2011), Clear-sky biases in satellite infra-red estimates of upper tropospheric humidity and its trends, *J. Geophys. Res.*, *116*, D14108, doi:10.1029/2010JD015355.

John V. O., G. Holl, S. A. Buehler, B. Candy, R. W. Saunders, and D. E. Parker (2012a), Understanding inter-satellite biases of microwave humidity sounders using global simultaneous nadir overpasses, *J. Geophys. Res.*, *117*(D2), D02305, doi:10.1029/2011JD016349.

John V. O., R. P. Allan, B. Bell, S. A. Buehler, and A. Kottayil (submitted 2012b), Assessment of inter-calibration methods for satellite microwave humidity sounders, *J. Geophys. Res.*, available online at http://www.sat.ltu.se/publications/?bibkey=johnxx:_assessment_jgr#top.

Karbou F., F. Aires, C. Prigent, and L. Eymard (2005), Potential of advanced microwave sounding unit-A (AMSU-A) and AMSU-B measurements for atmospheric temperature and humidity profiling over land, *J. Geophys. Res.*, *110*(D07109), doi:10.1029/2004JD005318.

Labrot T., L. Lavanant, K. Whyte, N. Atkinson, and P. Brunel (2011), AAPP documentation scientific description, version 7.0, Tech. Rep. NWPSAF-MF-UD-001, Numer. Weather Predict. Satell. Appl. Facil., Exeter, U. K.

Liu Q., and F. Weng (2005), One-dimensional variational retrieval algorithm of temperature, water vapor, and cloud water profiles from advanced microwave sounding unit (AMSU), *IEEE T. Geosci. Remote*, *43*(5), 1087–1095.

Saunders R. W., T. J. Hewison, S. J. Stringer, and N. C. Atkinson (1995), The radiometric characterization of AMSU-B, *IEEE T. Microw. Theory*, *43*(4), 760–771.

Shi L., and J. J. Bates (2011), Three decades of intersatellite-calibrated High-Resolution Infrared Radiation Sounder upper tropospheric water vapor, *J. Geophys. Res.*, *116*, D04108, doi:10.1029/2010JD014847.

Shi L., J. J. Bates, and C. Y. Cao (2008), Scene radiance-dependent intersatellite biases of HIRS longwave channels, *J. Atmos. Oceanic Technol.*, *25* (12), 2219–2229, doi:10.1175/2008JTECHA1058.1.

Sreerekha T. R., S. A. Buehler, U. O'Keeffe, A. Doherty, C. Emde, and V. O. John (2008), A strong ice cloud event as seen by a microwave satellite sensor: Simulations and observations, *J. Quant. Spectrosc. Radiat. Transfer*, *109*(9), 1705–1718, doi:10.1016/j.jqsrt.2007.12.023.

Wang L., C. Cao, and P. Ciren (2007), Assessing NOAA-16 HIRS radiance accuracy using simultaneous nadir overpass observations from airs, *J. Atmos. Oceanic Technol.*, *24*, 1546–1561, doi:10.1175/JTECH2073.1.

Weng F., R. R. Ferraro, and N. C. Grody (1999), Effects of AMSU-A cross track asymmetry of brightness temperatures on retrieval of atmospheric and surface parameters, in Microw. Radiomet. Remote Sens. Earth's Surf. Atmosphere, edited by P. Pampaloni and S. Paloscia, pp. 255–262.

Weng F., L. Zhao, R. R. Ferraro, G. Poe, X. Li, and N. C. Grody (2003), Advanced microwave sounding unit cloud and precipitation algorithms, *Radio Sci.*, *38*(4), 8068, doi:10.1029/2002RS002679.

Xavier P. K. (2012), Intraseasonal convective moistening in CMIP3 models, *J. Climate*, *25*, 2569–2577, doi:http://dx.doi.org/10.1175/JCLI-D-11-00427.10.

Xavier P. K., V. O. John, S. A. Buehler, R. S. Ajayamohan, and S. Sijikumar (2010), Variability of Indian summer monsoon in a new upper tropospheric humidity data set, *Geophys. Res. Lett.*, *37*, L05705, doi:10.1029/2009GL041861.

Zou C.-Z., and W. Wang (2011), Intersatellite calibration of AMSU-A observations for weather and climate applications, *J. Geophys. Res.*, *116*, D23113, doi:10.1029/2011JD016205.